ORIGINAL ARTICLE

Effect of tool path on cutting force in end milling

Kaining Shi[1] · Ning Liu[2] · Sibao Wang[3] · Junxue Ren[1]

Abstract

Tool path generation is an important task in end milling. In the existing literature, the tool path pattern/style is determined based on geometric analysis. However, there is little analysis from the viewpoint of machining dynamics/cutting force, which is more related to the final manufacturing performance. Although there are many types of tool paths (e.g., zigzag, spiral, and ISO-scallop tool path), they can be decomposed into a number of circular tool paths with various path radii and cutting angles. Firstly, by investigating chip formation mechanism, the effect of tool path radius on uncut chip thickness is obtained. Analysis shows that tool path radius has a significant influence on uncut chip thickness, thus affecting the cutting force, especially when the tool path radius is small. Then, the effect of cutting angle on cutting force distribution is analyzed. It is found that the feed direction could vary the distribution of cutting force in X and Y direction in 3-axis end milling. Based on such analysis, the cutting force prediction model considering tool path effect is established. To validate the proposed model, various experiments have been carried out based on well-designed tool paths. The comparative results show that (1) tool path has great effect on cutting force through the tool path radius, rotation direction, and start/end point, and (2) the proposed model is capable of providing accurate cutting force prediction considering tool path effect. From a physical viewpoint, the proposed method provides huge potential in automated/intelligent tool path optimization towards better surface quality via minimizing cutting force, which significantly contributes to the state of the art in tool path generation.

1 Introduction

End milling is widely used in aerospace, die, and mold manufacturing industry [1]. One of the main concern in end milling is tool path generation/optimization to achieve the desired objectives [2]. The tool path not only determines the tool movement distance and moving time [3] but also directly affects the chip formation during the machining process. From a geometric view, different tool paths will produce different machined surface topology; from a physical view, they will lead to different machined surface quality/integrity [4]. In the existing literature, extensive research has been conducted to generate/optimize tool path to improve the machined surface quality. Via geometric analysis, the spiral tool path is smoothed to guarantee G1 continuous and avoid overcut/undercut [5]. A real-time interpolation strategy for line segments consists of a transition scheme that is proposed to make sure the G2 continuity [6]. Based on geometric characteristics of the error regions, the ISO-scallop tool path is generated by comparing the digitized manufactured surface with the designed surface [7]. On basis of linear-piecewise path, the 5-axis flank milling tool path is optimized towards minimum geometric error [8]. To avoid the interference and reduce cutter posture variation, an optimized tool path is generated in 5-axis machining of centrifugal impeller with split blades [9].

Kaining Shi and Ning Liu contributed equally to this work.

✉ Sibao Wang
   wangsibaocqu@cqu.edu.cn

   Kaining Shi
   shikaining@nwpu.edu.cn

   Ning Liu
   liuning@u.nus.edu

1 School of Mechanical Engineering, Northwestern Polytechnical University (NPU), Xi'an 710072, Shaanxi, People's Republic of China

2 Department of Mechanical Engineering, National University of Singapore, 9 Engineering Drive 1, Singapore 117576, Singapore

3 State Key Laboratory of Mechanical Transmission, Department of Mechanical Engineering, Chongqing University, 174 Shazheng Street, Chongqing 400044, China

Similarly, to avoid the interference in five-axis sculptured surface machining, a smooth tool path is generated by constructing cutter's accessibility map [10]. To minimize the machining error in the end milling of thin-wall workpiece, the tool path is optimized by adjusting the cutter location [11]. Similarly, to minimize the machining error in flank milling, a tool path is planned using an ant colony system by mapping two boundary curves of a ruled surface [12]. Considering the chord error by proper feedrate scheduling, a time-optimal tool path is generated for five-axis computer numerical control machining [13]. Recently, the tool path patterns are compared to increase the machining efficiency in robotic milling [14]. Variable depth of cut multi-pass tool path is generated for the sculptured surface machining to improve machining efficiency in multi-axis machining[15].

These studies have successfully improved the machined surface topology. However, most of them investigate the effect of tool path from a geometric viewpoint. Therefore, it may not be sufficient as the physical nature of machining process is not thoroughly considered in the tool path generation/optimization. To address this problem, some researchers have tried to study the effect of tool path on the machining process from a physical viewpoint to optimize tool path towards better surface quality. For example, a tool path with constant cutting force is generated in the direction parallel milling [16]. However, the study is based on an incorrect assumption that the cutting force is only determined by material remove rate; in fact, the cutting force is affected by many machining parameters such as depth of cut, spindle speed, and feedrate [17, 18]. Based on linear tool path assumption, the cutting force with the effect of tool path is directly computed from computer aided manufacturing files [19]. Further, multiple objectives including the cutting force and scallop height are considered in tool path optimization based on mean cutting force calculation from linear tool movement [20]. These studies have improved the tool path generation from machining dynamics with the simple linear tool path movement. However, it has been revealed that the tool path radius has great effect on the cutting force from the experimental [21] and complicated analytical study [22] in end milling. Even for linear tool path, feed direction or cutting angle also has great effect on the cutting force [23]. Comparisons are done for the linear tool path, sinusoidal tool path, descending sawtooth tool path, ascending sawtooth tool path, and triangle tool path experimentally [24]. By measuring the generated mean cutting force and surface roughness, results show that the triangle and sinusoidal tool path generate smaller cutting force and better surface roughness compared with the other types of tool path, while the cutting time is almost the same. The effect of various tool path styles on cutting force and tool deflections is studied in machining of inclined surface [25]. Three kinds of tool paths are experimentally compared in terms of tool life and tool wear [26]. Although current research has provided a guideline

for the manufacturer to select proper tool path from the physical viewpoint, it is mainly based on an experimental method, which is usually time consuming and expensive. Therefore, it is necessary to analytically investigate the effect of tool path, in order to further optimize tool path towards desired cutting force variation and machined surface quality.

Although there are many types of tool path strategies (e.g., zigzag, spiral, ISO-planar tool path, and ISO-scallop tool path), they can be classified into two categories according to the tool path trajectory, i.e., linear and circular tool paths defined by tool path radius and feed direction. In this study, the effect of tool path radius on uncut chip thickness is studied by introducing the instantaneous feed per tooth, and the feed direction affects cutting force by varying the cutting force distribution in X and Y direction. Based on such analysis, the cutting force considering the effect of tool path can be predicted. With the proposed cutting force prediction model considering tool path effect, tool path optimization can be better achieved from a physical viewpoint, which provides huge potential in automated/intelligent tool path generation. Thus, the study can significantly advance the state of the art in the topic of tool path generation. The paper is organized as follows. In Section 2, the definition of linear/circular tool path in end milling is presented. Section 3 presents the cutting force prediction model considering the effect of tool path. In Section 4, various well-designed experiments have been carried out to validate the proposed cutting force prediction model in end milling. Finally, Section 5 concludes the study.

2 Definition of the tool path in end milling

Characterized by trajectory, tool path can be classified into linear tool path and circular tool path as shown in Fig. 1. The linear tool path is determined by feed direction defined by cutting angle Φ as shown in Fig. 1a. The cutting angle is measured from the X-axis under the right-hand rule. The circular tool path is determined by the circular path radius R and feed direction Φ of a cutting point **P** as shown in Fig. 1b. The
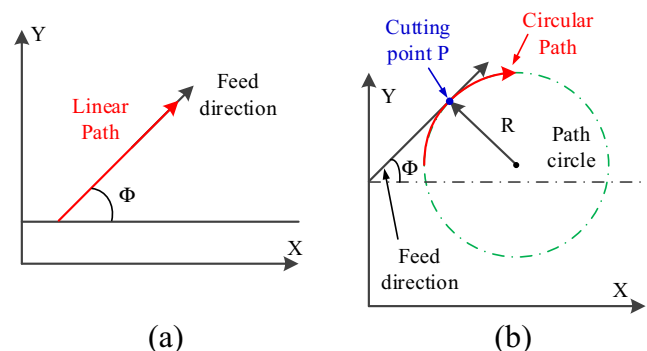

Fig. 1 Definition of a tool path. **a** Linear path. **b** Circular path
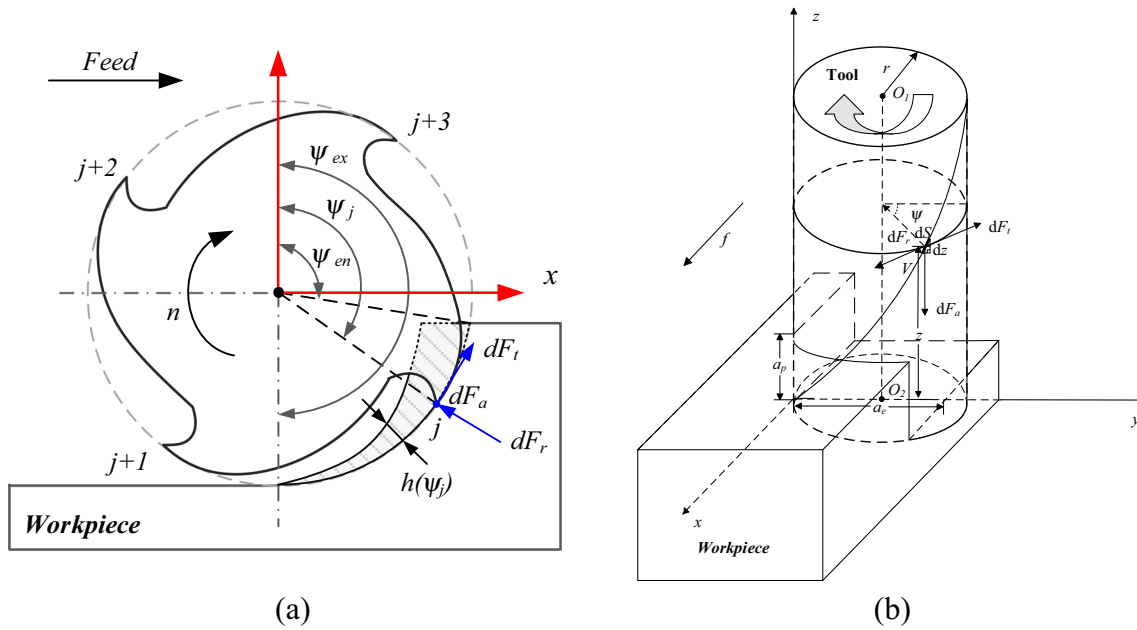
Fig. 2 Cutting force prediction in end milling. **a** Top view. **b** Iso-metric view [29]

feed direction is determined by cutting position and rotation direction of the circular tool path. It should be noted that the linear tool path can be considered as a circular tool path with infinite path radius, all the tool path types can be seen as a circular tool path with various tool path radii and feed directions/angles.

3 Cutting force prediction considering the effect of tool path

The cutting force prediction considering the effect of tool path is based on the cutting force prediction model under ideal condition, which is shortly presented in Section 3.1. As all the tool paths can be seen as circular tool path defined by circular path radius R and feed direction Φ, the effect of tool path on cutting force will be decomposed into two parts: (1)

the effect of circular path radius on cutting force and (2) the effect of feed direction on cutting force. The feed direction affects the cutting force by varying the distribution of the resultant cutting force as presented in Section 3.2, while the circular path radius affects the cutting force by varying the instantaneous uncut chip geometry as presented in Section 3.3.

3.1 Cutting force prediction under linear movement

In this section, the cutting force prediction under linear movement is presented in the cutter coordinate system (CCS) O_T-$X_T Y_T Z_T$ (see Fig. 2). The cutter is discretized into N layers and the flutes on each layer undergo oblique cutting. The cutting force generated by each elemental cutting edge is decomposed into tangential, radial, and axial force in the local coordinate, denoted as dF_t, dF_r, and dF_a, which is obtained by:

$$dF_t = K_{te}dz + K_{tc}h(\psi)dz \tag{1a}$$

$$dF_r = K_{re}dz + K_{rc}h(\psi)dz \tag{1b}$$

$$dF_a = K_{ae}dz + K_{ac}h(\psi)dz \tag{1c}$$

where K_{te}, K_{re}, K_{ae} and K_{tc}, K_{rc}, K_{ac} are the edge force coefficients and the shear force coefficients which can be obtained either by experimental calibration [27] or mechanistic calculation [18]; $h(\psi)$ is the uncut chip thickness (UCT); ψ is the angular location of any cutting edge element which is calculated by Eq. 2 (refer to [28] for more details).

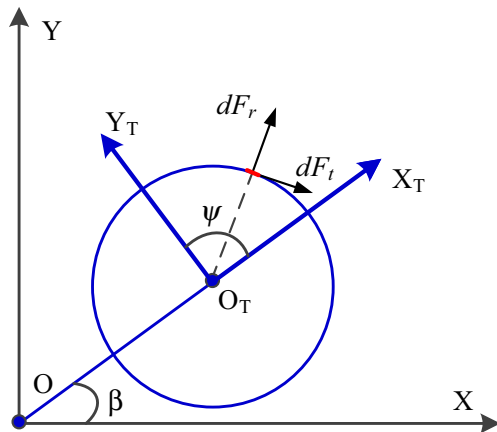$$\psi = \theta + (i-1)\phi_p - \phi_z \tag{2}$$

Fig. 3 Effect of feed direction on cutting force

To get the cutting force acting on the cutter, the elemental cutting force in the local coordinate should be transformed into the cutter's frame, which is obtained by:

$$dF_{xyz}^{CCS} = T_1 dF_{tra} \tag{3}$$

where $dF_{tra} = [dF_t \ dF_r \ dF_a]^{\mathrm{T}}$, $dF^{CCS}_{xyz} = [dF^{CCS}_x \ dF^{CCS}_y \ dF^{CCS}_z]^{\mathrm{T}}$, and T_1 is the transformation matrix from local coordinate to the cutter's frame, and is obtained by:

$$T_1 = \begin{bmatrix} -\sin(\psi) & -\cos(\psi) & 0 \\ -\cos(\psi) & \sin(\psi) & 0 \\ 0 & 0 & -1 \end{bmatrix}$$

The total cutting force is obtained by integrating the elemental cutting force generated by the engaged cutting edges at the current time instant, which is expressed as:

$$\begin{pmatrix} F_x^{CCS} \\ F_y^{CCS} \\ F_z^{CCS} \end{pmatrix} = \sum_{i=1}^{N} \int \begin{pmatrix} dF_x^{CCS} \\ dF_y^{CCS} \\ dF_z^{CCS} \end{pmatrix} \tag{4}$$

3.2 Effect of feed direction on cutting force

Generally, the stiffness of machine tool system in X or Y direction is not the same, i.e., the stiffness of the machine tool system is anisotropy [30]. Therefore, regardless of the measurement or analysis of the cutting force, it should be determined in the workpiece coordinate system (WCS) $O\text{-}XYZ$ as WCS is fixed in the machine tool. Meanwhile, the feed direction may vary depending on machining requirements, which will affect the cutting force distribution. The effect of feed direction on cutting force is shown in Fig. 3. With the effect of feed direction, the cutting force produced by any elemental cutting edge should be transformed into WCS from CCS, which can be obtained by:
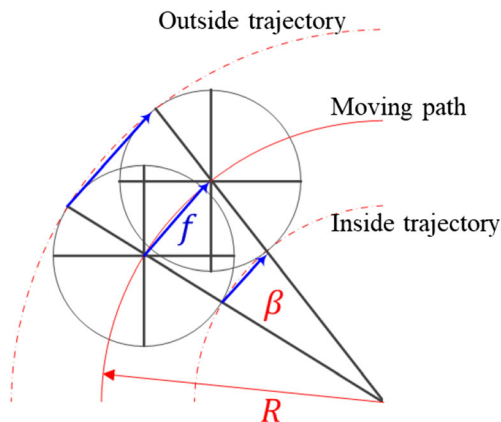
$$dF_{xyz} = T_2 T_1 dF_{tra} \tag{5}$$

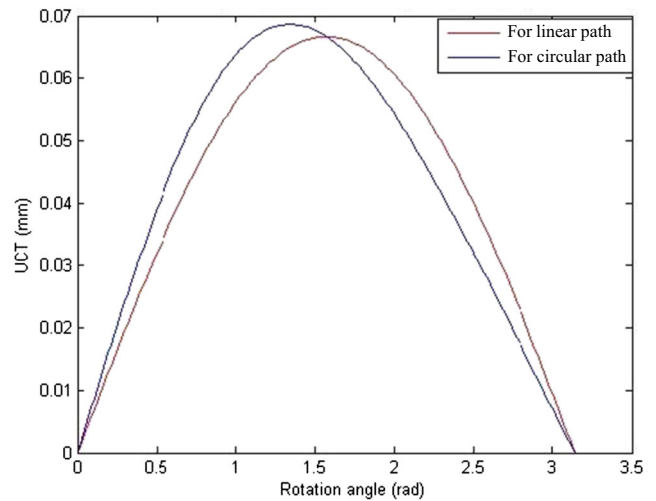Fig. 4 Effect of tool path radius on uncut chip geometry

Fig. 5 Comparison of the uncut chip thickness between linear and circular tool path

Here, $dF_{xyz} = [dFx \ dFy \ dFz]$ is the elemental cutting force in WCS. T_2 is the transformation matrix from $X_{\mathrm{T}}\text{-}Y_{\mathrm{T}}\text{-}Z_{\mathrm{T}}$ coordinate to $X\text{-}Y\text{-}Z$ frame and $T_2 = [\cos(\beta) \ \sin(\beta) \ 0; \ \sin(\beta) \ \cos(\beta) \ 0; \ 0 \ 0 \ 1]$. The total cutting force in WCS can be obtained by Eq. 4.

3.3 Effect of tool path radius on uncut chip geometry

The effect of tool path radius on uncut chip geometry is illustrated in Fig. 4. UCT varies with different elemental cutting edges as the instantaneous feed per tooth changes. The instantaneous feed per tooth for each elemental cutting edge can be obtained by:

$$f(\psi) = \beta * r(\psi) \tag{6}$$

where β is the increased cutter rotation angle along the designed tool path obtained by $\beta = f / R$; $r(\psi)$ is the instantaneous
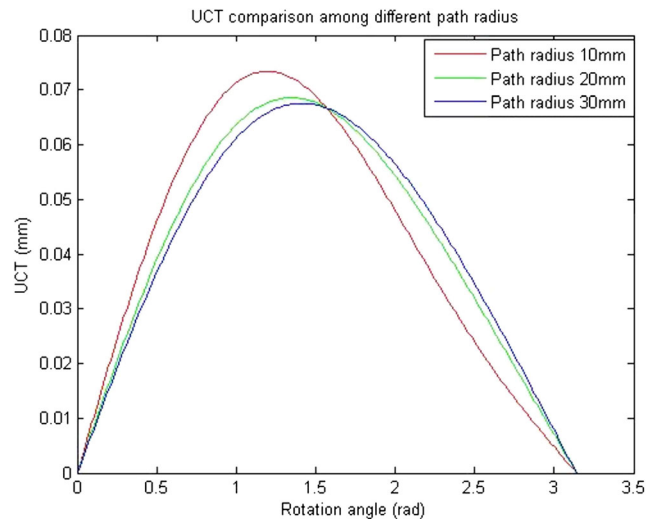

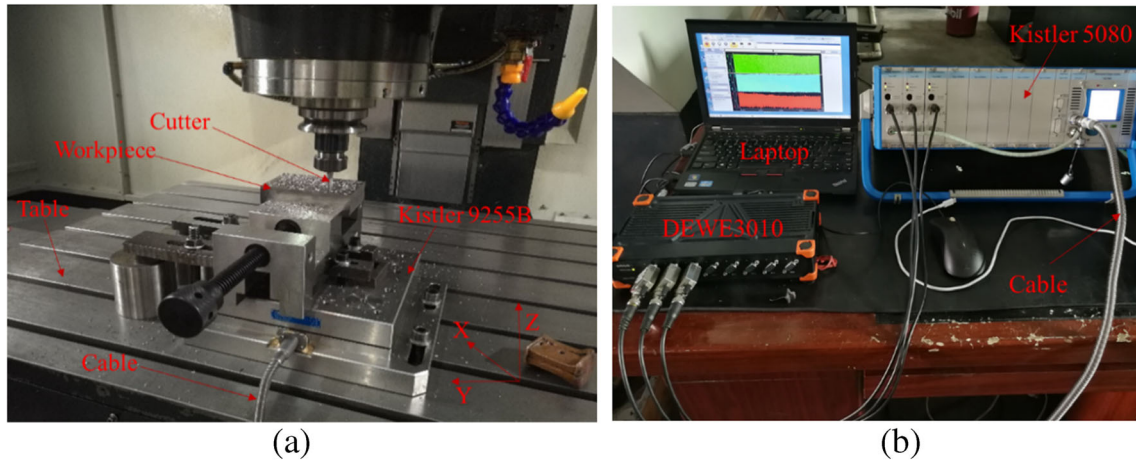Fig. 6 Effect of tool path radius on the uncut chip thickness

Fig. 7 Experimental setup. **a** Machine tool and setup. **b** Dynamometer

moving radius obtained by $r(\psi) = r_0 + r_0\cos(\psi)$; f is the designed feed per tooth; r_0 is the radius of the milling cutter. UCT is obtained by:

$$h(\psi) = f(\psi)*\sin(\psi) \tag{7}$$

It is clear that f is constant for each elemental cutting edge in linear tool path (circular path with infinite radius), and UCT is obtained by $h(\psi) = f * \sin(\psi)$. This comforts with the one in most of the current research based on the assumption that the cutter is moving along linear tool path.

From Eqs. 6 and 7, it can be seen that tool path radius affects UCT by changing the instantaneous feed per tooth. To clearly visualize this effect, the UCT comparison between the linear and circular tool path is shown in Fig. 5. In this example, the designed feed per tooth is 0.066 mm for both linear and circular tool paths, and the circular path radius is 20 mm. The UCTs for linear and circular tool paths are obviously different in amplitude and phase. Furthermore, the effect of different circular path radii on the UCT is also studied. The

UCT comparison among different path radii (i.e., 10 mm, 20 mm, and 30 mm) is shown in Fig. 6. It can be seen that the effect of path radius will be more significant when the path radius is smaller. Therefore, the effect of path radius can be neglected only when the circular path radius is large enough.

So far, we have modeled the effect of tool path radius on uncut chip geometry and studied the effect of feed direction on cutting force distribution. The final cutting force with the effect of tool path can be determined by combining Eqs. (1), (4), (5), and (7). The complete algorithm works as follows:

Stage 1. For each tool path, it is decomposed into several circular tool paths. The radius and feed direction are determined based on the tool path information.
Stage 2. At each time instant, UCT is obtained by Eq. 7 considering the effect of circular path radius.
Stage 3. The elemental cutting force obtained by Eq. 1 is transformed into WCS according to Eq. 5.
Stage 4. The final cutting force is obtained by summing up all the elemental cutting force generated by the engaged cutting edges using Eq. 4.
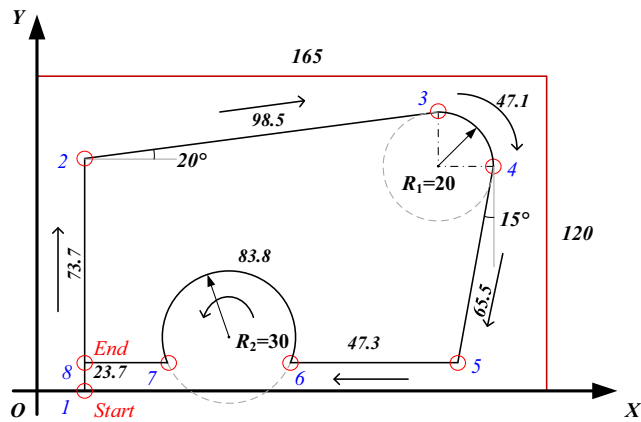

Fig. 8 Designed tool path for the experiments

Table 1 Experimental conditions

No.	a_p [mm]	n [rpm]	v_f [mm/min]
1	0.2	1500	200
2	0.2	2000	300
3	0.2	2500	400
4	0.4	1500	300
5	0.4	2000	400
6	0.4	2500	200
7	0.6	1500	400
8	0.6	2000	200
9	0.6	2500	300

Table 2 Calibrated cutting force coefficients

k_{tc} (N/mm^2)	k_{rc} (N/mm^2)	k_{ac} (N/mm^2)	k_{te} (N/mm)	k_{re} (N/mm)	k_{ae} (N/mm)
1282.31	579.16	− 487.43	4.34	5.38	− 6.79

4 Experimental validation

4.1 Experimental details

Various experiments have been carried out to validate the proposed model considering the tool path effect on cutting force in end milling. The experimental setup details are shown in Fig. 7. The machine tool is LEADWELL MCV-1500i+, a 3-axis CNC vertical milling center. Solid carbide flat-end cutters are used under dry cutting condition. The 2-flute cutters have a helix angle 40° and a radius 5 mm. The workpiece is a cuboid with a dimension of 165 mm × 60 mm × 42 mm. Its material is aluminum alloy 7050, a type of alloy that is extensively used in aerospace industry. To experimentally validate the effect of tool path radius and feed direction on cutting force, specific tool path is designed as shown in Fig. 8. The milling cutter starts cutting from point 1, cuts the workpiece along a linear path or circular path to pass through points 2–7, and stops at point 8. The well-designed tool path includes various feed directions and circular path radii. The tool path is carried out under various machining conditions as shown in Table 1. Throughout the machining experiment, cutting force is measured by Kistler 9255B. The sample rate is 20,000 Hz. To remove the effect of noise, the low pass filtering is adopted and set as 500 Hz. It should be noted that the experiment is assumed under stable machining process.

4.2 Results and discussion

The calibrated cutting force coefficients are presented in Table 2 using the method in [31]. Based on them, the predicted

and measured cutting forces under different tool paths are compared. For the linear tool paths 1-2, 2-3, 4-5, and 5-6, the cutting force in any circle would be the same. Therefore, the cutting force comparison is only meaningful in one circle instead of the whole tool path. Figure 9a and b show the comparison result and prediction error in a cycle for tool path 1-2 whose feed direction is 90°. The prediction error δ_p is the absolute deviation between the measured and predicted force at a cutter rotation angle, i.e., $\delta_p = |F_{\text{measured}} - F_{\text{predicted}}|$. For tool path 1-2, the maximum prediction error is smaller than 3.5 N, which is quite small. The comparative results show a good agreement between the experimental and predicted results considering the effect of cutting angle. To further study the effect of feed direction on cutting force, the other feed directions are also used in tool paths 2-3, 4-5, and 5-6, respectively. Figures 10, 11, and 12 show the comparative result in a cycle for tool paths 2-3, 4-5, and 5-6, respectively. As can be seen, the prediction errors in these tool paths (i.e., 1.8 N, 2 N, and 3 N) are very small, clearly showing effectiveness of the proposed method (Table 3).

Tool paths 3–4 and 6–7 are the circular tool paths with different path radii. Therefore, they are chosen to investigate the effect of tool path radius on the cutting forces. The comparison between the measured and predicted cutting force for tool path 3-4 whose feed direction varies from 0° to − 90° is shown in Fig. 13. It is clear that the predicted results accurately match the measured results. The maximum prediction error is as small as 3 N. Furthermore, with the effect of path radius and feed direction variation, the cutting force in X direction F_x monotonically increases, while the cutting force in Y direction F_y slightly increases first and then decreases. As F_x varies
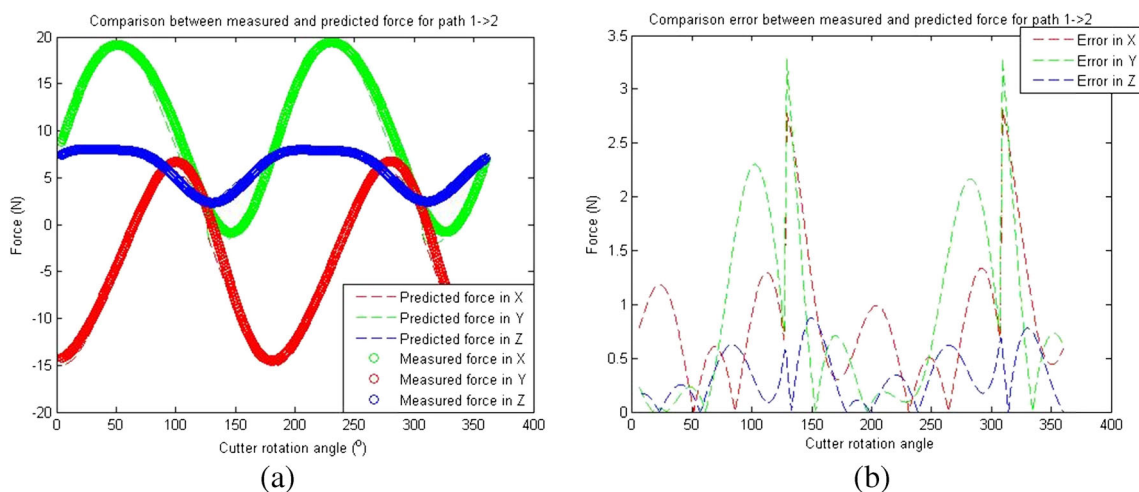

Fig. 9 Comparison between the measured and predicted force for path 1-> 2. **a** Force comparison. **b** Prediction error
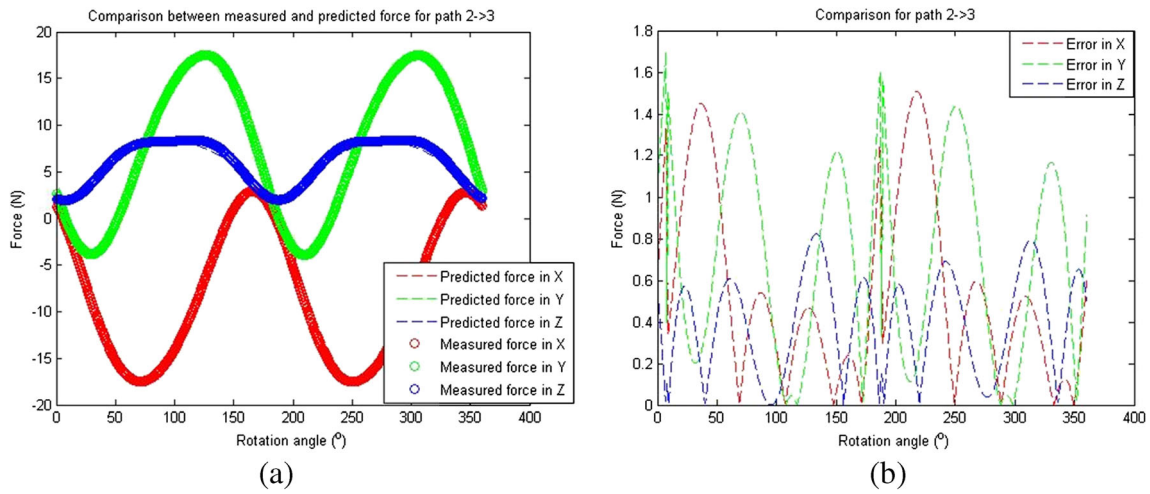
Fig. 10 Comparison between the measured and predicted force for path 2-> 3. **a** Force comparison. **b** Prediction error
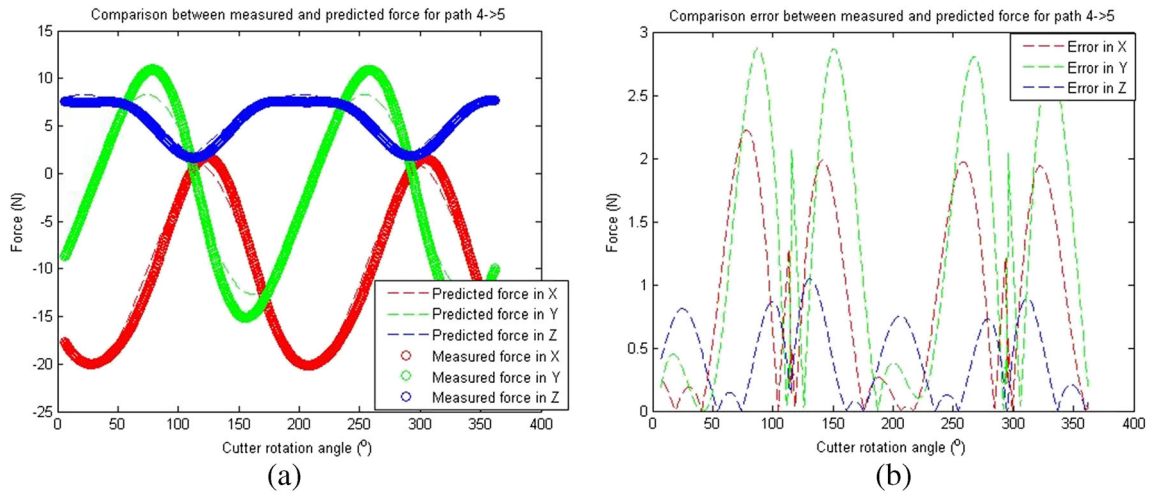

Fig. 11 Comparison between the measured and predicted force for path 4-> 5. **a** Force comparison. **b** Prediction error

from negative to positive, it implies that proper feed angle (50° in this circular tool path) can be determined to reduce the amplitude of F_x. With the smallest $|F_x|$, the deflection in X direction will be minimized. This would be beneficial if
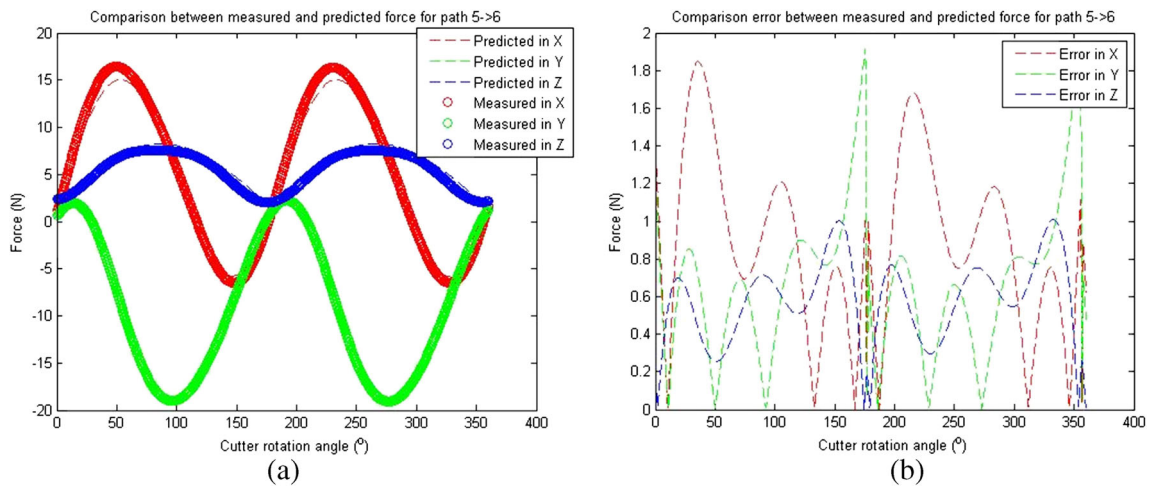

Fig. 12 Comparison between the measured and predicted force for path 5-> 6. **a** Force comparison. **b** Prediction error

Table 3 Feed direction for linear tool path

Path number	Tool path 1-2	Tool path 2-3	Tool path 4-5	Tool path 5-6
Cutting angle	90°	20°	255°	180°

deflection in X direction is of more concern, e.g., workpiece in X direction is a thin wall. Another tool path 6-7 is used to compare the predicted results with measured results in a large circular rotation angle with different tool path radii, as shown in Fig. 14. It can be seen that F_x increases first and then suddenly decreases, while F_y decreases first and then increases. Similarly, if the deflection in Y direction is of more concern, the feed direction with tool path radius 30 mm should be 230° to minimize the amplitude of F_y.

The tool path is characterized by the path radius, start/end point, and path rotation direction (clockwise/anti-clockwise). Even the tool path radius is the same, and different start/end

points and path rotation directions may generate different tool paths. An example is shown in Fig. 15. The cutter travels between **A** and **B** with a given path radius 30 mm. Three paths can be obtained under different start/end points and path rotation angles as shown in Fig. 15. It is clear that the feed direction angle is changing from 0° to −90° in CPath1, 90° to 180° in CPath2, and 270° to 360° in CPath3. The cutting force under the three tool paths is compared as shown in Fig. 16. As the cutting force variation in Z direction is small, it is neglected in the comparison results. It can be observed that the tool path rotation direction and start/end point clearly affect the final cutting force. The first comparison is presented
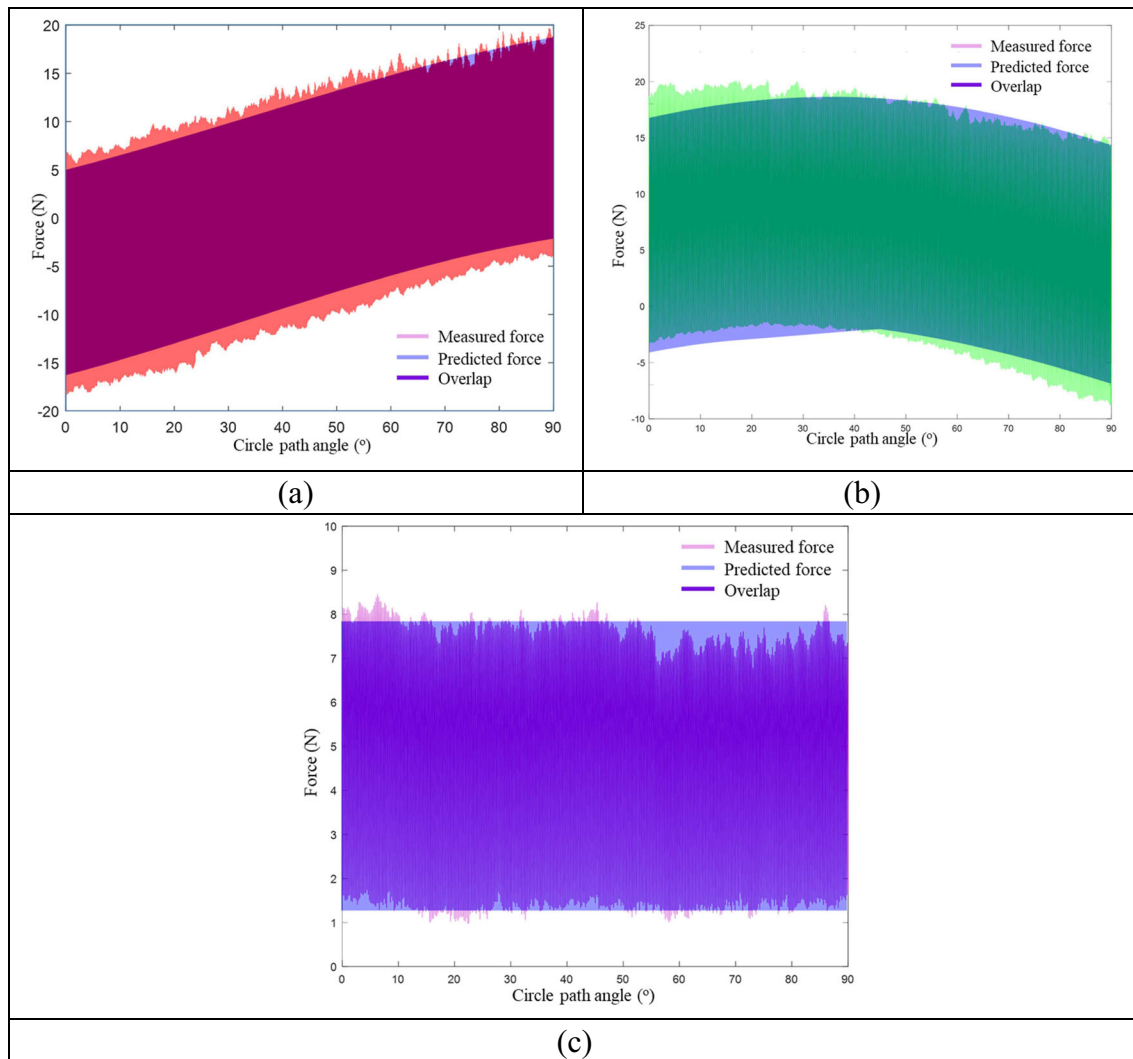

Fig. 13 Comparison between the measured and predicted force for path 3-> 4. **a** Comparison in X direction. **b** Comparison in Y direction. **c** Comparison in Z direction
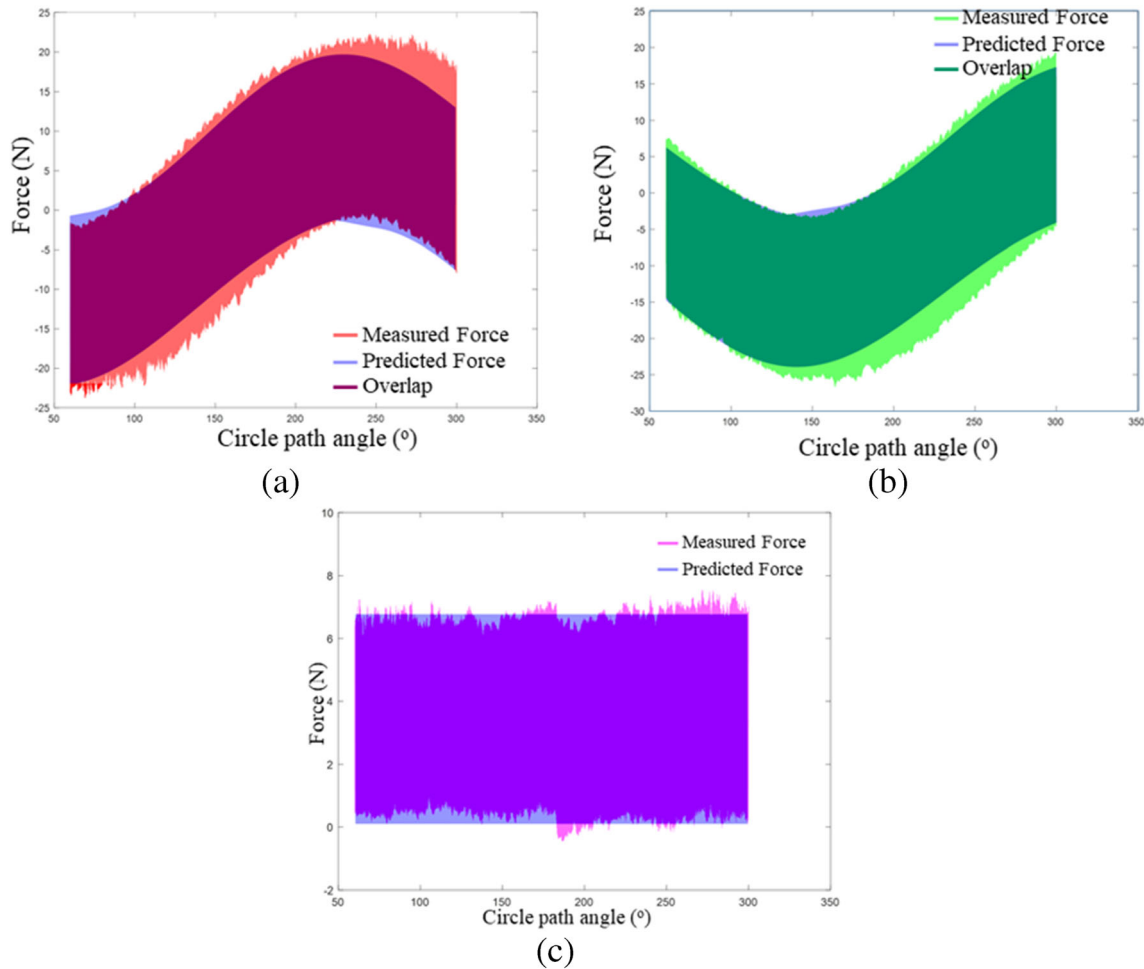
Fig. 14 Comparison between the measured and predicted force for path 6-> 7. **a** Comparison in *X* direction. **b** Comparison in *Y* direction. **c** Comparison in *Z* direction

between CPath1 and CPath2. They look the same but with interchanged start/end points. From the comparison results shown in Fig. 16a–d, it can be observed that the distribution and amplitude of cutting forces for the two paths are quite different. From a geometric viewpoint, CPath1 and CPath2 will produce the same machined topography. However, as the generated cutting forces are different, the machined

surface quality shall differentiate from each other. The second comparison is presented between CPath1 and CPath3. The rotation radii and start/end points are the same, but rotation directions are different (clockwise and anti-clockwise). As can be seen from the comparison, the F_x for CPath1 varies from negative to positive (see Fig. 16a), while the F_x for CPath2 varies in an opposite way (see Fig. 16e). In the comparison
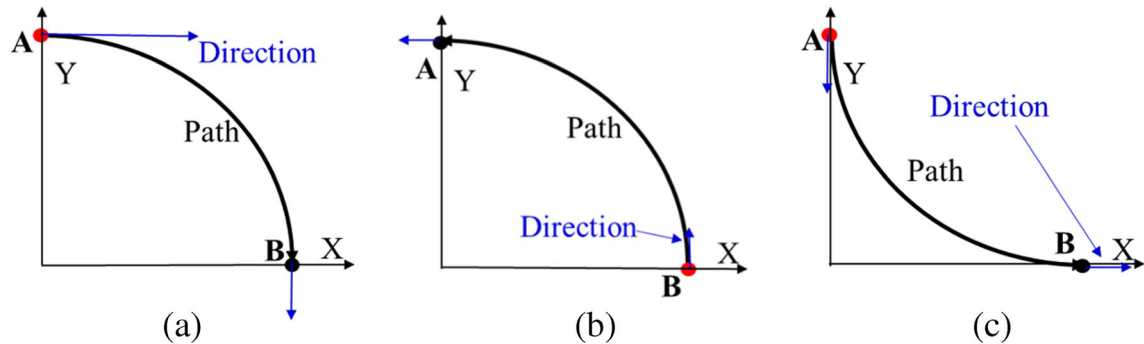

Fig. 15 Comparison under the effect of path direction. **a** CPath1. **b** CPath2. **c** CPath3
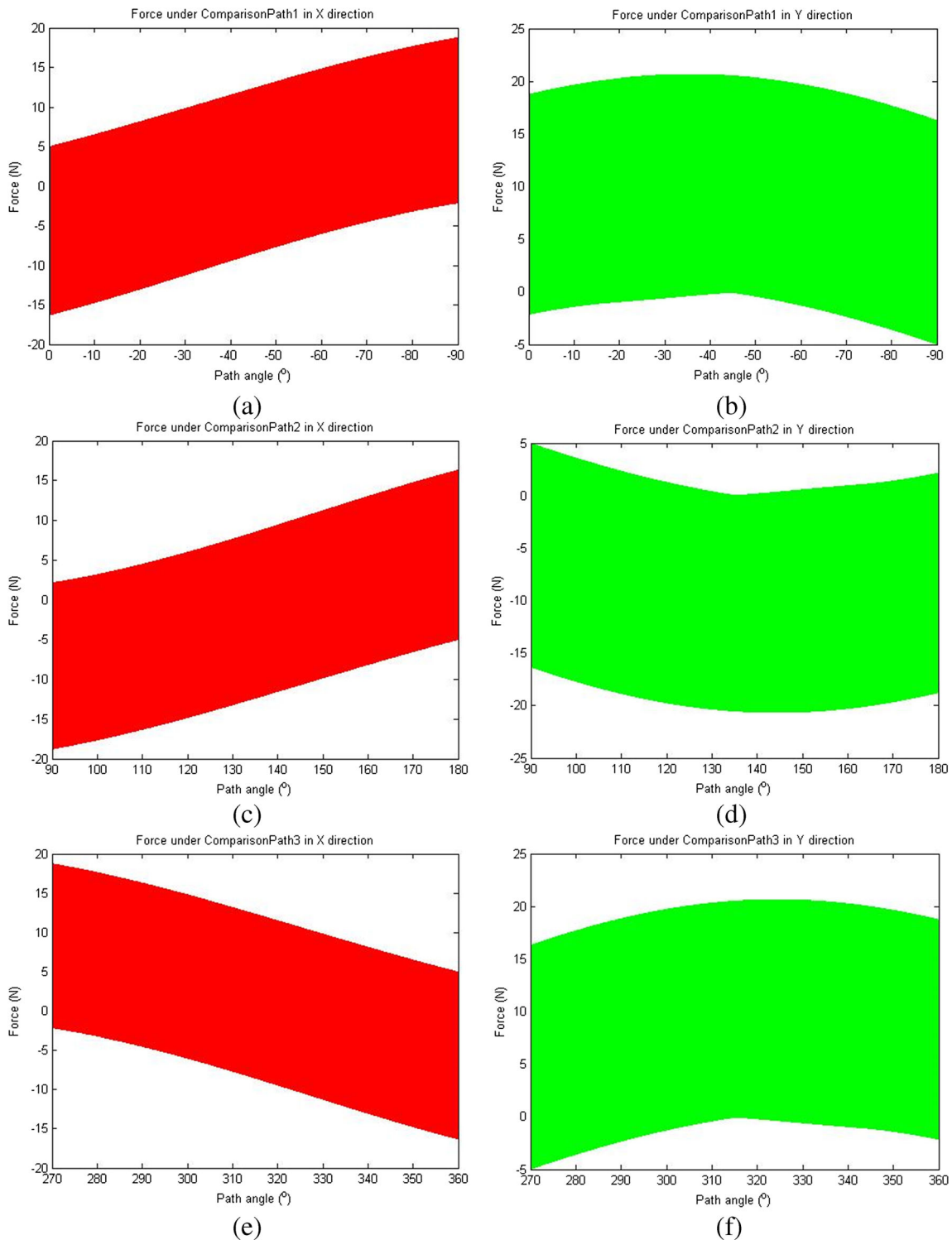
Fig. 16 Comparison between three conditions under the same path radius. **a** F_x for CPath1. **b** F_y for CPath1. **c** F_x for CPath2. **d** F_y for CPath2. **e** F_x for CPath3. **f** F_y for CPath3

between CPath2 and CPath3, the rotation directions are the same (anti-clockwise), while the start/end point and feed direction are different. The generated cutting forces by the two paths are significantly different in both X and Y direction (see Fig. 16c, d). To summarize, these three comparative studies reveal that the tool path parameters (i.e., rotation direction, rotation radius, and start/end point) have great influence on cutting forces. In the future work, based on the proposed method, the tool path will be optimized to reduce the cutting force by adjusting these tool path parameters.

5 Conclusions

This paper studies the effect of tool path on cutting force, which is quite important for tool path optimization from a physical viewpoint. All the current tool path strategies are decomposed into a series of circular tool path with different path radii (radius of the linear tool path can be seen as infinite) and feed direction. The tool path radius affects cutting force by influencing the uncut chip thickness, while the feed direction affects cutting force by changing the cutting force distribution. Finally, the proposed cutting force prediction method considering the effect of tool path is validated by various experiments. Some interesting conclusions can be obtained:

1) When the tool path radius is smaller, its effect on uncut chip thickness is greater.
2) The cutting force in X and Y direction is greatly varied by feed direction. This implies that the feed direction can be well adjusted to minimize the cutting force in the desired direction, which is quite useful for thin-wall machining.
3) The start/end point, rotation direction, and path radius of a tool path greatly affect the cutting force by changing the uncut chip thickness and cutting force distribution.

From a physical viewpoint, the proposed method provides huge potential in automated/intelligent tool path optimization towards better surface quality via minimizing cutting force, which significantly advances to the state of the art in tool path generation.

In the future work, the thermal behavior of material will be considered to improve the prediction accuracy. In addition, the tool path optimization from physical viewpoint will be carried out to achieve the desired cutting force and machined surface quality.

References

1. Zhu K, Zhang Y (2017) Modeling of the instantaneous milling force per tooth with tool run-out effect in high speed ball-end milling. Int J Mach Tools Manuf 118–119:37–48
2. Li L, Deng X, Zhao J, Fu Z, Sutherland JW (2018) Multi-objective optimization of tool path considering efficiency, energy-saving and carbon-emission for free-form surface milling. J Clean Prod 172:3311–3322
3. Geng L, Zhang YF, Fuh JYH (2011) A neural network based approach to 5-axis tool-path length estimation for optimal multi-cutter selection. Comput Aided Des Appl 8(2):301–313
4. Geng L, Liu PL, Liu K (2015) Optimization of cutter posture based on cutting force prediction for five-axis machining with ball-end cutters. Int J Adv Manuf Technol 78(5-8):1289–1303
5. Held M, Spielberger C (2009) A smooth spiral tool path for high speed machining of 2D pockets. Butterworth-Heinemann 41(7):539–550
6. Hui W, Wu J, Chao L, Xiong Z (2018) A real-time interpolation strategy for transition tool path with C2 and G2 continuity. Int J Adv Manuf Technol 98(1-4):905–918
7. Lasemi A, Xue D, Gu P (2012) A freeform surface manufacturing approach by integration of inspection and tool path generation. Int J Prod Res 50(23):6709–6725
8. Chu CH, Wu PH, Lei WT (2012) Tool path planning for 5-axis flank milling of ruled surfaces considering CNC linear interpolation. J Intell Manuf 23(3):471–480
9. Chu CH, Huang WN, Li YW (2012) An integrated framework of tool path planning in 5-axis machining of centrifugal impeller with split blades. J Intell Manuf 23(3):687–698
10. Li LL, Zhang YF, Li HY, Geng L (2011) Generating tool-path with smooth posture change for five-axis sculptured surface machining based on cutter's accessibility map. Int J Adv Manuf Technol 53(5-8):699–709
11. Wan XJ, Hua L, Wang XF, Peng QZ, Qin XP (2011) An error control approach to tool path adjustment conforming to the deformation of thin-walled workpiece. Int J Mach Tools Manuf 51(3):221–229
12. Tien KW (2011) Efficient tool path planning for 5-axis flank milling of ruled surfaces using ant colony system algorithms. Int J Prod Res 49(6):1557–1574
13. Fan W, Gao XS, Lee CH, Zhang K, Zhang Q (2013) Time-optimal interpolation for five-axis CNC machining along parametric tool path based on linear programming. Int J Adv Manuf Technol 69(5-8):1373–1388
14. Tunc LT, Stoddart D (2017) Tool path pattern and feed direction selection in robotic milling for increased chatter-free material removal rate. Int J Adv Manuf Technol 89(9):2907–2918
15. Chen L, Li Y, Tang K (2018) Variable-depth multi-pass tool path generation on mesh surfaces. Int J Adv Manuf Technol 95(5-8):2169–2183
16. Kim HC (2011) Tool path generation and modification for constant cutting forces in direction parallel milling. Int J Adv Manuf Technol 52(9-12):937–947
17. Wang SB (2015) Automated five-axis tool path generation based on dynamic analysis. PHD Thesis National University of Singapore, Singapore.
18. Shi KN, Wang SB, Liu N, Ren JX, Yuan Y (2019) Experimental and theoretical investigation of milling tool selection towards energy-efficient process planning in discrete parts manufacturing. Int J Adv Manuf Technol. https://doi.org/10.1007/s00170-019-03960-3
19. Zeroudi N, Fontaine M, Necib K (2012) Prediction of cutting forces in 3-axes milling of sculptured surfaces directly from CAM tool path. J Intell Manuf 23(5):1573–1587
20. Manav C, Bank HS, Lazoglu I (2013) Intelligent toolpath selection via multi-criteria optimization in complex sculptured surface milling. J Intell Manuf 24(2):349–355
21. Banerjee A, Bordatchev EV (2012) Effect of circular tool path on cutting force profile in micro-end-milling. Arch Proc Inst Mech Eng Part C J Mech Eng Sci 1989-1996 (vols 203-210) 226(6):1589–1600
22. Kardes N, Altintas Y (2007) Mechanics and dynamics of the circular milling process. J Manuf Sci Eng 129(1):21–31
23. Ma JW, Hu GQ, Jia ZY, Zhang N, Wang FJ (2018) Effect of geometric feature and cutting direction on variation of force and vibration in high-speed milling of TC4 curved surface. Int J Adv Manuf Technol 95(5-8):2207–2218
24. Da Silva RHL, Hassui A (2018) Cutting force and surface roughness depend on the tool path used in side milling: an experimental investigation. Int J Adv Manuf Technol 96(1-4):1445–1455

25. Gok A, Gologlu C, Demirci HI (2013) Cutting parameter and tool path style effects on cutting force and tool deflection in machining of convex and concave inclined surfaces. Int J Adv Manuf Technol 69(5-8):1063–1078

26. Toh CK (2003) Tool life and tool wear during high-speed rough milling using alternative cutter path strategies. Proc Inst Mech Eng B J Eng Manuf 217(9):1295–1304

27. Shi KN, Zhang DH, Liu N, Wang SB, Ren JX, Wang SL (2018) A novel energy consumption model for milling process considering tool wear progression. J Clean Prod 184:152–159

28. Liu N, Zhang YF, Lu WF (2015) A hybrid approach to energy consumption modelling based on cutting power: a milling case. J Clean Prod 104:264–272

29. Shi KN, Ren JX, Wang SB, Liu N, Liu ZM, Zhang DH, Lu WF (2019) An improved cutting power-based model for evaluating total energy consumption in general end milling process. J Clean Prod 231:1330–1341. https://doi.org/10.1016/j.jclepro.2019.05.323

30. Wang S, Geng L, Zhang Y, Liu K, Ng TE (2016) Chatter-free cutter postures in five-axis machining. Proc Inst Mech Eng Part B J Eng Manuf 230:1428–1439

31. Wang S, Geng L, Zhang Y, Liu K, Ng TE (2015) Cutting force prediction for five-axis ball-end milling considering cutter vibrations and run-out. Int J Mech Sci 96:206–215. https://doi.org/10.1016/j.ijmecsci.2015.04.007